Chemical Engineering Journal 250 (2014) 25–34

Contents lists available at ScienceDirect

Chemical Engineering Journal

journal homepage: www.elsevier.com/locate/cej

Surface treatment effects on CO oxidation reactions over Co, Cu, and Ni-doped and codoped CeO_2 catalysts

Yohan Park [a], Seog K. Kim [a], Debabrata Pradhan [b], Youngku Sohn [a,*]

[a] *Department of Chemistry, Yeungnam University, Gyeongsan 712-749, Republic of Korea*
[b] *Materials Science Centre, Indian Institute of Technology, Kharagpur 721 302, W.B., India*

HIGHLIGHTS

- Co, Cu, and Ni-doped and codoped CeO_2 catalysts were prepared.
- CO oxidation was tested over as-prepared and thermal-treated the catalysts.
- Cu-contained CeO_2 commonly showed higher catalytic activity after thermal treatment in N_2 atmosphere.
- Charge balance of doped metals appears to play a major role.

GRAPHICAL ABSTRACT

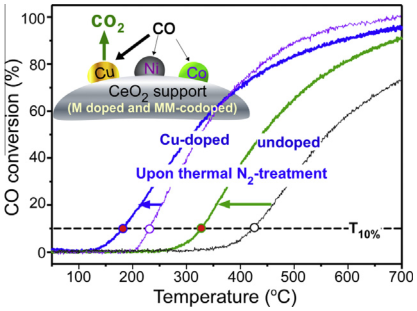

ARTICLE INFO

Article history:
Received 6 December 2013
Received in revised form 13 March 2014
Accepted 20 March 2014
Available online 28 March 2014

Keywords:
CeO_2
CO oxidation
Metal-doping
Co-doping
Thermal-pretreatment

ABSTRACT

We doped (M) and codoped (MM') Co, Cu, and Ni into CeO_2 support, and tested their gas-phase CO oxidation performance by temperature-programmed reaction mass spectrometry for the as-prepared, thermal H_2- and N_2-treated samples. Additionally, fundamental characteristics of doped CeO_2 were revealed by transmission electron microscopy, optical microscopy, X-ray diffraction crystallography, UV–visible absorption, Brunauer–Emmett–Teller (BET) surface area measurements, and temperature-programmed reduction experiments. The CO oxidation performance was greatly improved upon metal-doping and thermal pre-treatment in H_2 and N_2 condition. It was found that Cu-contained samples showed higher CO performance while Ni, Co and CoNi-doped samples showed poor performances. The $T_{10\%}$ (the temperature at 10% CO conversion) was lowered by 140 °C upon Cu-doping. Upon N_2 (or H_2-thermal treatment), the $T_{10\%}$ was lowered by 80 and 110 °C for Cu-doped and undoped CeO_2 catalyst, respectively. Overall, this study provides deeper information of surface treatment effects useful to development of efficient catalysts.

1. Introduction

Efficient conversion from one molecule to another is very important for the chemical synthetic industry and clean environments. This efficiency increases drastically when an efficient catalyst is used during the conversion processes. Developing catalysts for efficient CO oxidation to less toxic CO_2 has been of great interest for reducing air pollution [1–28]. Among many metal oxides investigated as potential candidates for catalyst support, cerium (IV) oxide (CeO_2) has been widely employed as a typical model system due to the unique behavior of its convertible oxidation states (Ce^{4+}/Ce^{3+}) by accepting and releasing oxygen [1,2,29–34]. Accordingly, CeO_2 has been employed to understand oxidation pathways, in which surface oxygen and defects plays roles in oxidation reactions [35–39]. The morphology-controlled synthesis of catalyst

---

* Corresponding author. Tel.: +82 53 810 2354; fax: +82 53 810 4613.
E-mail address: youngkusohn@ynu.ac.kr (Y. Sohn).

http://dx.doi.org/10.1016/j.cej.2014.03.070
1385-8947/

and/or its support is another important factor in the catalysis. Therefore, extensive efforts have been devoted to synthesize CeO_2 with various morphologies from wires to cubes [40–46]. Furthermore, transition metals (e.g., Au, Ag and Pd) have commonly been introduced into oxide supports to obtain a drastic enhancement of catalytic effect [1,2,4–28,47–49]. Doping cheap transition metals such as Cu, Co and Ni has been shown to be useful for generation of catalysts for CO oxidation and steam reforming reactions [1,21–24,47–53]. Cu–CeO_2 has been reported to be superior for CO oxidation than Ni and Co-doped CeO_2 catalysts [1,50]. Bera et al. attributed the higher CO oxidation activity of Cu-loaded CeO_2 to two redox couples of Cu^{2+}/Cu^{+} and Ce^{4+}/Ce^{3+} [51]. Additionally, the interactions between Cu and vacant oxygen were found to enhance chemical reactivity and the formation of oxygen vacancies [52]. Moreover, Co–CeO_2 and Ni–CeO_2 catalysts were shown to be more efficient for steam reforming reactions than CO oxidation [47–49]. Additionally, investigation of Ni–CeO_2 catalyst used for steam reforming of ethanol revealed that metallic Ni initially helps adsorption of ethanol, while Ce^{3+} acts as a site for decomposing water [48].

In this study, we doped three (Cu, Co and Ni) different metals and codoped two different (CoCu, CoNi, CuNi,) metals into CeO_2 support and then investigated whether there was a hybrid synergic effect in gas-phase CO oxidation reactions before and after thermal-treatment with and without H_2-condition. The CO oxidation reactions commonly occur at the gas/solid interface via a simplified $CO + [O]^{*}–CeO_2 \rightarrow CO_2 + CeO_2$ process. Although low temperature CO oxidation studies have extensively been performed we further disclose a major role of doped and codoped metals that boosts or negates a catalytic oxidation reaction. Moreover, the originality of the present paper is quantitatively to show the influence of thermal treatment effects on CO oxidation over the various doped and codoped CeO_2 catalysts.

2. Experimental

2.1. Catalyst preparation

For preparation of all catalysts, we employed a hydrothermal method in a 100 mL Teflon-lined stainless autoclave. We first prepared 0.1 M cerium(III) nitrate hexahydrate (99%, Aldrich, USA), cobalt(II) nitrate hexahydrate (97%, Samchun, Korea), nickel(II) nitrate hexahydrate (98%, Samchun, Korea), and copper(II) nitrate trihydrate (99%, Daejung, Korea) solutions, after which we added an appropriate amount of each solution to ammonia solution (28–30%, Samchun, Korea) for precipitation. The total doped metal concentration was then fixed at 5 mol% (the corresponding weight% is summarized in Table 1 below), after which the mixed solution was transferred into the Teflon-lined stainless autoclave, and placed at 200 °C for 12 h. Upon finishing the reaction, the sample was allowed to cool naturally, after which the precipitates were washed and dried in an oven at 80 °C overnight. The prepared catalysts were 5 mol% Co (1.77 wt%), Cu (1.76 wt%), Ni-doped (1.91 wt%) CeO_2 powder, and 2.5/2.5 mol% Co/Cu (0.88/0.95 wt%), Cu/Ni (0.95/0.88 wt%), and CoNi-codoped (0.88/0.88 wt%) CeO_2 powder.

2.2. Catalyst characterization

The crystal structures of the powder samples were examined using a PANalytical X'Pert Pro MPD diffractometer with Cu Kα radiation. The morphology of the samples was examined by transmission electron microscopy (TEM) using a Hitachi H-7600 operated at 100 kV and optical microscopy. Diffuse reflectance spectra for the powder samples were obtained using a Cary 5000 UV–Vis spectrophotometer. Raman spectra were obtained using a Bruker Senterra Raman spectrometer with a laser excitation energy of 532 nm. Fourier-transform infrared (FT-IR) measurements were taken using a Thermo Scientific Nicolet iS10 spectrometer.

2.3. Catalytic performance tests

Temperature programmed reduction experiments were performed at a heating rate of 20 K/min under 5% H_2/N_2 flow with a flow rate of 40 mL/min. For CO oxidation experiments, we used as-prepared catalysts without high temperature calcination, and thermal-treated samples at 450 °C in 5% H_2/N_2 flow condition for 2 h. For the selected samples (undoped and Cu-doped CeO_2 catalysts) we also annealed to 450 °C in N_2 flow condition and then cooled to ambient temperature before the CO oxidation test. The CO oxidation experiments were conducted under $CO(1.0\%)/O_2/(2.5\%)/N_2$ flow conditions with a flow rate of 40 mL/min and a heating rate of 20 K/min. The final gas products were detected using a quadrupole mass spectrometer (RGA200, Stanford Research Systems). The amount of catalysts was 10 mg for the CO oxidation experiment.

3. Results and discussion

3.1. Morphology

Fig. 1 shows the SEM, TEM and optical microscopy images of the doped CeO_2 catalysts. Compared to the SEM and TEM image (not shown) of undoped CeO_2, the morphology was not critically changed upon metal doping. The TEM images revealed that the particle sizes were very similar, but that each sample showed a unique color due to absorption of different doped metals. Upon doping with Co, Cu and Ni, the pale ivory color of undoped CeO_2 changed to light brown, green and yellow, respectively, as shown in the insets of Fig. 1. For the codoped samples, the color appeared as a mix of two different colors. To more clearly show the particle sizes, we obtained size distribution profiles of the doped CeO_2 samples. For undoped CeO_2, the average particle size was found to be around 16 nm, while the sizes (11–14 nm) were slightly smaller for the doped samples. The particle sizes were calculated from the XRD patterns and discussed compared with the sizes obtained from the TEM images below.

Table 1

Calculated XRD crystalline sizes, TEM sizes, and BET surface areas (m^2/g) of undoped (reference) CeO_2, doped (Co, Cu, and Ni) and co-doped (CoCu, CoNi, and CuNi) CeO_2 catalysts. The mol and weight% of doped metals are also summarized.

Dopants	Undoped	Co	Cu	Ni	CoCu	CoNi	CuNi
mol%	–	5	5	5	2.5/2.5	2.5/2.5	2.5/2.5
wt%	–	1.77	1.76	1.91	0.88/0.95	0.88/0.88	0.95/0.88
Crystalline Size (nm)	18.0	12.3	12.3	16.1	13.3	14.7	14.3
TEM size	16.1	11.4	12.3	13.0	13.4	13.2	13.1
Surface area (m^2/g)	56.4	68.0	68.2	58.0	65.4	61.0	61.6

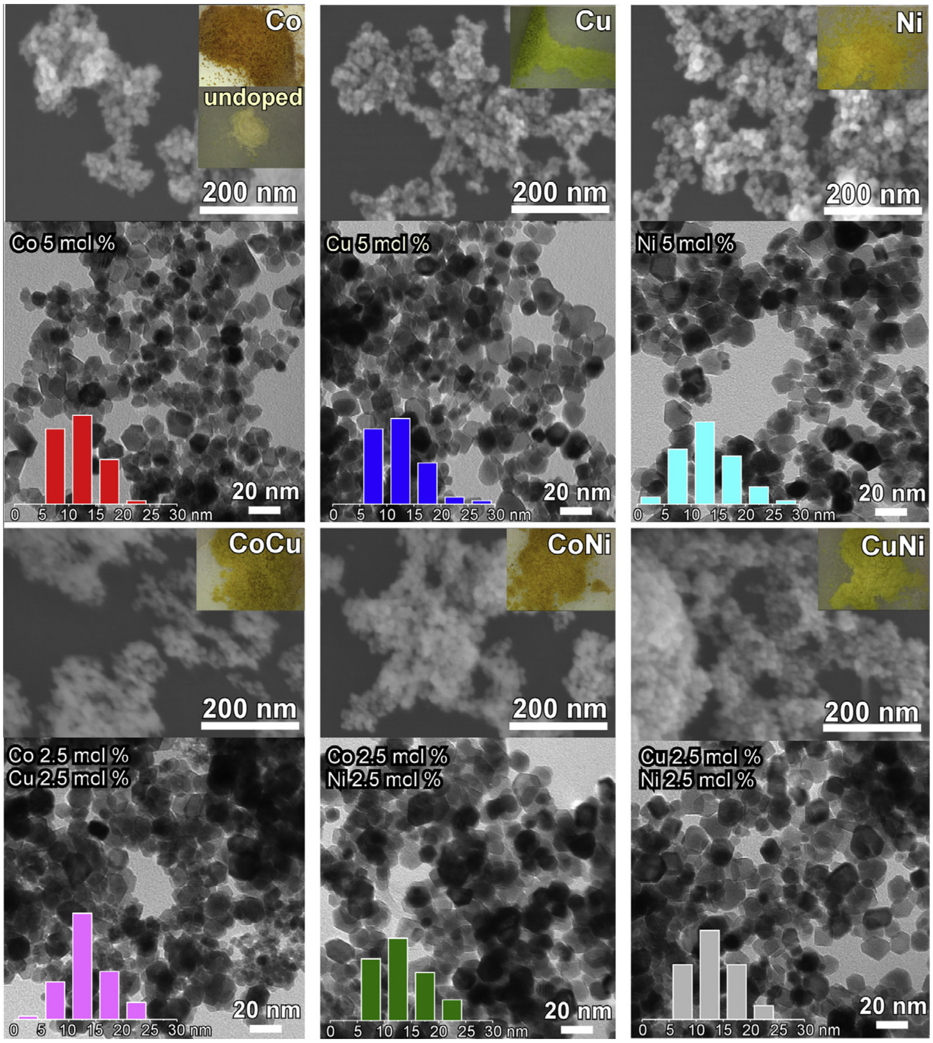

Fig. 1. SEM and TEM images of doped (Co, Cu, and Ni = 5 mol%) and co-doped (CoCu, CoNi, and CuNi = 2.5/2.5 mol%) CeO_2 catalysts. The optical microscopy images are shown as inset of corresponding TEM images. The optical microscopy image of undoped CeO_2 is below that of Co-doped CeO_2. The lower left inset shows the size distribution profile of the corresponding TEM image.

3.2. Crystal structures, sizes, and surface areas

We employed XRD to ascertain the change in bulk crystal structure for CeO_2 support. Fig. 2 displays the XRD patterns and the corresponding crystal planes of the catalysts. The 2θ values were located at 28.5°, 33.1°, 47.4°, 56.2°, 59.0°, and 69.4° for the undoped CeO_2. The peak positions showed no critical change upon doping with guest metals, indicating that the cell lattice parameters were not changed. It is not clear that this reflects no solid solution formation [8]. All peaks matched those of the cubic (Fm-3m) structure (JCPDS 034-0394, $a = b = c = 5.41$ Å) of CeO_2 well and were assigned to the (111), (200), (220), (311), (222), and (400) planes, respectively. The relative I(111)/I(200) revealed no critical differences between samples, indicating that the exposed crystal planes were very similar. The XRD results imply that the small amount of quest metals did not critically change the bulk crystalline structure of the metal oxide support. We found no XRD peaks corresponding doped metals or their oxides. This could indicate that the doped metals were uniformly dispersed in the CeO_2 matrix [8]. Otherwise, they are amorphous or undetectable amount by XRD. To derive the particle sizes from the broadness of the XRD peak, we took the strongest peak corresponding to the (111) plane at $2\theta = 28.5°$ and measured the full-width at half

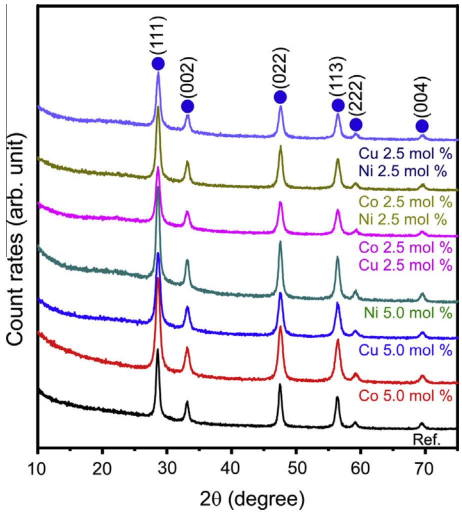

Fig. 2. Powder X-ray diffraction patterns of reference CeO_2, doped (Co, Cu, and Ni) and co-doped (CoCu, CoNi, and CuNi) CeO_2 catalysts. The major crystal planes are shown on the peaks.

maximum. The sizes were calculated to range from 18.0 to 12.3 nm using Scherrer's equation (Table 1). While the undoped CeO_2 had a size of 18.0 nm, the Cu and Co-doped CeO_2 samples were 12.3 nm. As summarized in Table 1, the calculated particles sizes were fairly in good agreement with the average particle sizes obtained from the TEM size distribution profile (Fig. 1).

We measured the BET surface areas based on the N_2 adsorption and desorption profiles. The surface area of the undoped sample was estimated to be 56.4 m^2/g, while the surface areas increased slightly upon doping, possibly due to a decrease in size. For Ni and Cu-doped samples, we obtained surface areas of 58.0 and 68.2 m^2/g, respectively. We expected the largest surface area for the Co and Cu-doped samples based on the calculated crystalline sizes and the TEM average particle sizes which are summarized in Table 1.

3.3. Optical absorption bandgaps

The UV–visible absorption spectra of undoped CeO_2, doped (Co, Cu, and Ni) and co-doped (CoCu, CoNi, and CuNi) CeO_2 catalysts are displayed in Fig. 3. Although the absorption data was not closely related with the catalytic activity this further confirms metal doping into CeO_2. The inset photographs show the colors of the corresponding powder samples. The absorbance (Y-axis) was converted from the diffuse reflectance by the Kubelka–Munk method. To estimate the direct bandgap transition, we replotted the absorbance spectra with $(\alpha h\nu)^2$ versus $h\nu$, where α is the absorption coefficient and the $h\nu$ is photo energy in eV. The absorption edge (or the bandgap) formed by the intersection of the two straight lines for the undoped CeO_2 was positioned at about 2.9 eV. The bandgap decreased upon doping, with the lowest value of ~2.0 eV being observed for the Co doped CeO_2.

3.4. Raman spectra

Fig. 4 displays the Raman spectra of reference CeO_2, as well as doped (Co, Cu, and Ni) and co-doped (CoCu, CoNi, and CuNi) CeO_2 catalysts. For CeO_2, a very strong peak appeared at 463 cm^{-1}, which was assigned to the F_{2g} mode of the cubic fluorite (Fm-3m) CeO_2 structure [5,54]. Upon doping and codoping with metal ions, the peak intensity decreased greatly and became red-shifted and broader, possibly due to poor crystallinity and a reduction in the particle size [27]. The reduction in size upon metal doping was evidenced by XRD and TEM (Table 1). The change in crystallinity and cell parameter was not detectable by XRD. The reduction in Raman peak is also plausibly due to the less scattered laser light because the UV–visible absorption at 532 nm (a wavelength of the Raman laser source) region was increased upon metal doping, especially for the Co-doped (Co, CoCu and CoNi) samples. For Cu–CeO_2 and CoCu–CeO_2 catalysts, the F_{2g} peaks were red-shifted by 8 and 22 cm^{-1}, respectively. The downshift of the F_{2g} Raman peak is known to be related to the concentration of oxygen vacancy [45]. As the vacancy is increased the reduction of Ce^{4+} to Ce^{3+} is more likely occurred to neutralize net charge. Since the atomic size of Ce^{3+} is larger than that of Ce^{4+} the lattice distance CeO_2 will be increased. The D (defect-induced mode) and 2LO (second order longitudinal optical mode) bands of undoped CeO_2 were found at 598 and 1167 cm^{-1}, respectively. These bands indicate the amount of surface oxygen vacancies. The bands became more pronounced and shifted to a lower wave number for Ni, Cu and CuNi-doped CeO_2 catalysts. It appears that Ni and CuNi-doped CeO_2 catalysts create more surface oxygen vacancies than Cu-doped CeO_2 catalyst. For other catalysts, the bands were less pronounced, possibly due to weak Raman intensity. It is not clear that the red-shift and reduction in Raman peak is also attributed to solid solution (dissolution of doped metals into CeO_2 support) formation such as CeM (M = Co, Cu, Ni)O_x. Actually, peak widths/shifts and the oxygen vacancy-related peaks showed no linear correlation with the CO oxidation activity. These findings indicate that the vacancy (or defect) does not solely determine the catalytic performance, but rather, that metal-oxide interactions (or the nature of doped metal) could play a significant role in the catalytic activity [55,56].

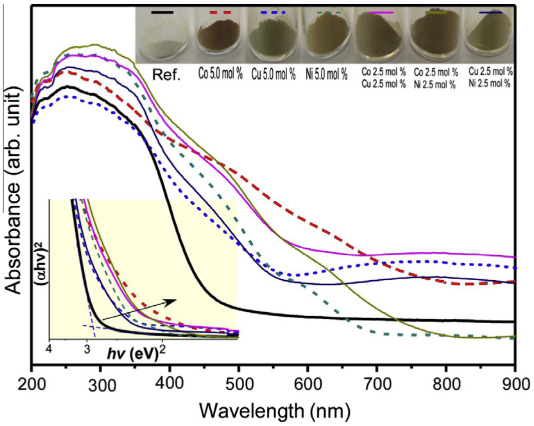

Fig. 3. UV–Visible diffuse reflectance absorption spectra of reference CeO_2, doped (Co, Cu, and Ni) and co-doped (CoCu, CoNi, and CuNi) CeO_2 catalysts. The top inset shows the photographs of the corresponding samples. The lower left inset shows the corresponding spectra displayed with $(\alpha h\nu)^2$ versus $h\nu$.

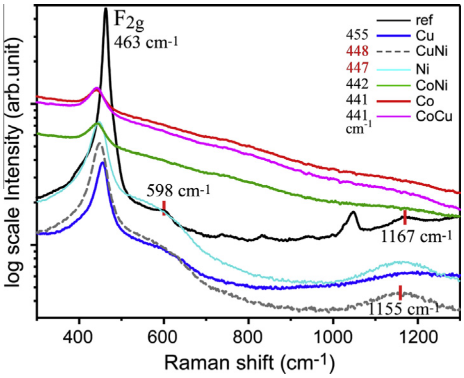

Fig. 4. Raman spectra (in log scale) of reference undoped CeO_2, doped (Co, Cu, and Ni) and co-doped (CoCu, CoNi, and CuNi) CeO_2 catalysts. Peak positions (F_{2g}) are shown on the right.

3.5. Hydrogen reduction properties

Temperature programmed hydrogen reduction (TPR) experiments were performed with a heating rate of 20 K/min and displayed in Fig. 5. For undoped reference CeO_2, two broad regions (near 600 °C and 900 °C) were observed in the TPR profile. The peak at 940 °C is generally attributed to the reduction ($Ce^{4+} \rightarrow Ce^{3+}$) of bulk CeO_2, while the former peak ~500 °C was due to reduction of surface oxygen of CeO_2 [4–6,14,57]. The bulk CeO_2 reduction peak was commonly observed at around 900 °C, with no significant change being observed for any samples. The surface reduction peak was changed significantly upon metal doping, and new peaks were appeared below 450 °C due to the reduction of doped metals [21,53,55]. All peaks were attributed to reduction of doped-metal oxides with different (e.g., weak and strong interactions with CeO_2 support) chemical environments [55]. The decrease in reduction peak of surface CeO_2 is due to doped-metal oxide clusters (e.g., solid solution and/or strongly interacted state) on the CeO_2 surface

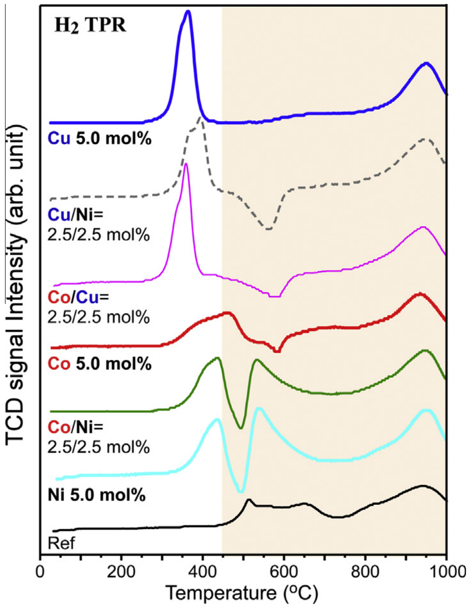

Fig. 5. Temperature-programmed H_2-reduction profiles of reference (undoped) CeO_2, doped (Co, Cu, and Ni) and co-doped (CoCu, CoNi, and CuNi) CeO_2 catalysts.

[8]. For Cu-doped CeO_2, a major peak at 362 °C and a weak shoulder at 347 °C were found. Razeghi et al. also reported a very similar TPR profile for CuO–CeO_2 catalyst prepared by a co-precipitation method [6]. The strong H_2-consumption peak was attributed to reduction of CuO (clustered and bulk) [6,27]. The Co-doped CeO_2 catalyst showed broader (but weaker) peaks at 406 °C and 462 °C. These two peaks were attributed to two-step reduction processes ($Co_3O_4 \rightarrow CoO$ followed by $CoO \rightarrow Co$) [28]. For the TPR of Ni-doped CeO_2, two broad peaks were clearly observed at 436 °C and 538 °C. In addition a negative peak was observed between the two peaks at around 500 °C. The former peak could be due to reduction of small NiO cluster species while the latter peak to strong NiO–CeO_2 reduction [28]. The negative peak is plausibly due to H_2 release by the decomposition of Ni hydride which was initially formed below 500 °C, or by Ni dissolution into CeO_2. For Ni-contained samples (Ni–CeO_2, CoNi–CeO_2 and CuNi–CeO_2), the negative peak was commonly observed. For the Cu-contained co-doped (CoCu and CuNi) samples, the profiles were very much similar to that of the Cu-doped sample. For the CoCu-doped sample, the peaks showed a major peak occurring at 359 °C and a weak shoulder at 337 °C. For the CuNi-codoped sample, the strong H_2-consumption peak slightly shifted to a higher temperature due to a stronger support interaction. The TPR of CoNi-doped sample resembled that of Ni-doped sample, and the feature of Co was not seen in the profile. We could not clearly discriminate an alloy state of two different metals in the TPR profiles for the co-doped samples, plausibly due to extremely low concentrations (<2 wt%) of coped metals.

3.6. Gas-phase CO oxidation performance for as-prepared samples

The CO oxidation over metal oxide catalysts has extensively been studied and well understood. Although the CO oxidation activity in the present study is lower than the literatures we further disclose the effect of doped metals pretreated at different conditions. Fig. 6 displays the first and second run CO conversion (%) profiles for the as-prepared undoped, doped (Co, Cu, and Ni), and co-doped (CoCu, CoNi, and CuNi) CeO_2 catalysts, as well as the corresponding Arrhenius plots (ln rate versus $1/T$). The activation energy (E_a) was measured in the CO conversion range of 10–15%, and valid only in the low conversion range, where the reaction rates are not critically affected by the heat or mass transfer limitations [19]. The reaction rate (v) was calculated using v = (CO flow rate, mol/s) × (CO conversion fraction)/(weight of the catalyst, g_{cat}) [23], where CO conversion fraction = $\{([CO]_{in} - [CO]_{out})/[CO]_{in}\}$. The $T_{10\%}$ (the temperature at 10% CO conversion), activation energies (E_a) and the difference values between the first and second CO oxidation runs are displayed in Fig. 7.

In the first CO oxidation run of undoped CeO_2, the $T_{10\%}$ was 428 °C. Upon doping with transition metals, the $T_{10\%}$ dramatically decreased by about 111–169 °C in the first runs. Based on the observed $T_{10\%}$, the CO oxidation activity with temperature occurred in the order of undoped (428 °C) $\ll$ Co (317 °C) $\approx$ Ni (314 °C) < CoNi (297 °C) < CuNi (284 °C) < CoCu (262 °C) $\approx$ Cu (259 °C) in the first run. The Cu-doped and CoCu-codoped CeO_2 showed CO oxidation activity at lower temperatures than the other samples. In the second runs, the CO oxidation occurred at much lower temperatures for all of the doped samples. This could be due to increased metal-support interactions after the first run. However, the CO oxidation activity of undoped CeO_2 did not change significantly. The CO oxidation activity occurred in the order of undoped (428 °C) $\ll$ Ni (302 °C) < Co (280 °C) < CoNi (264 °C) < CuNi (249 °C) < Cu (234 °C) < CoCu (206 °C) in the second run. The CoCu-codoped sample showed the lowest $T_{10\%}$ at 206 °C, which was 53 °C lower than that of the first run. Additionally, this $T_{10\%}$ was 222 °C lower than that of CeO_2. The CeO_2 catalysts containing Cu (CoCu, Cu and CuNi) generally showed better CO catalytic activity than other samples. Yakimova et al. tested the CO oxidation the performance of 5% M-CeO_2 (M = Cu, Co and Ni) catalyst, and found the order was undoped < Ni < Co < Cu [1,50]. The present study confirmed the reaction order in literatures. The activation energies (E_a) in the 1st run ranged from 105.0 to 77.7 kJ/mol. As shown in Fig. 7, the codoped samples showed lower values than other samples. In the 2nd run, the values were greatly reduced to 86.1–62.2 kJ/mol.

3.7. Gas-phase CO oxidation performance for H_2-treated and N_2-treated samples

We further tested CO oxidation performances for thermal (at 450 °C) H_2-treated undoped, doped (Co, Cu, and Ni), and co-doped (CoCu, CoNi, and CuNi) CeO_2 catalysts. The thermal-treatment temperature of 450 °C was the onset temperature of the surface oxygen reduction peak shown in the TPR profile of undoped CeO_2. At this temperature, it was assumed that all the doped metals were fully reduced. Fig. 8 shows the first and second run CO conversion (%) profiles and the corresponding Arrhenius plots for the H_2-treated catalysts. The corresponding $T_{10\%}$, activation energies (E_a) and the difference values between the first and second runs are displayed in Fig. 9. For comparing the as-prepared with the H_2-treated samples, we summarized the kinetic parameters in Table 2.

For the H_2-treated samples compared to the as-prepared samples, CO oxidation commonly occurred at lower temperatures. For the undoped CeO_2, $T_{10\%}$ was observed at 347 °C in the first run, which was 81 °C lower than that of the as-prepared sample. The $T_{10\%}$ was further lowered by 28 °C in the second run due to an enhanced crystallinity. For the H_2-treated metal-doped CeO_2 in the first run, the change in $T_{10\%}$ was not significant as that for undoped CeO_2. The $T_{10\%}$ of Co, Cu, Ni, CoCu, CoNi, and CuNi-doped CeO_2 catalysts were lowered by −44 °C, −52 °C, 0 °C, −31 °C, −50 °C and 2 °C, respectively compared with those of corresponding as-prepared samples in the first run. The differences in $T_{10\%}$ between the as-prepared and H_2-treated samples are plotted in Fig. 9 (bottom right) for the first and second runs. The Cu-contained samples commonly showed an good enhancement of CO oxidation performance while the Ni-contained samples showed a

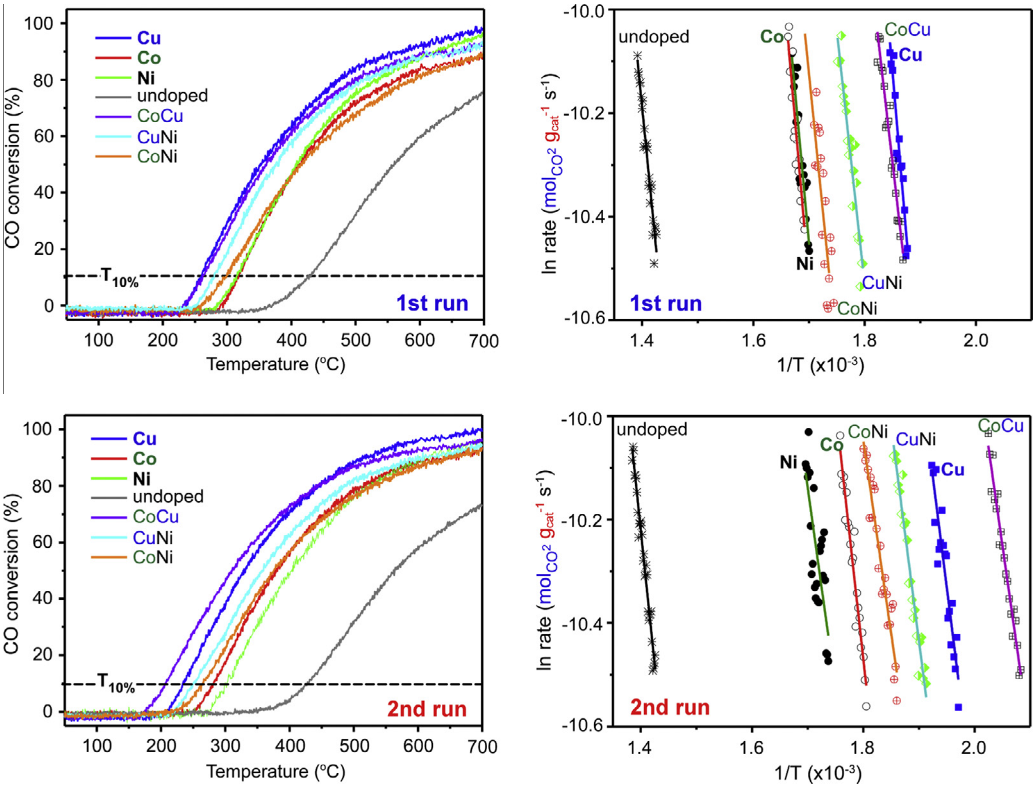

Fig. 6. Temperature programmed CO oxidation conversion (%) profiles (left two) and the corresponding Arrhenius plots (right two) for the first and second runs of reference (undoped) CeO_2, doped (Co, Cu, and Ni) and co-doped (CoCu, CoNi, and CuNi) CeO_2 catalysts.

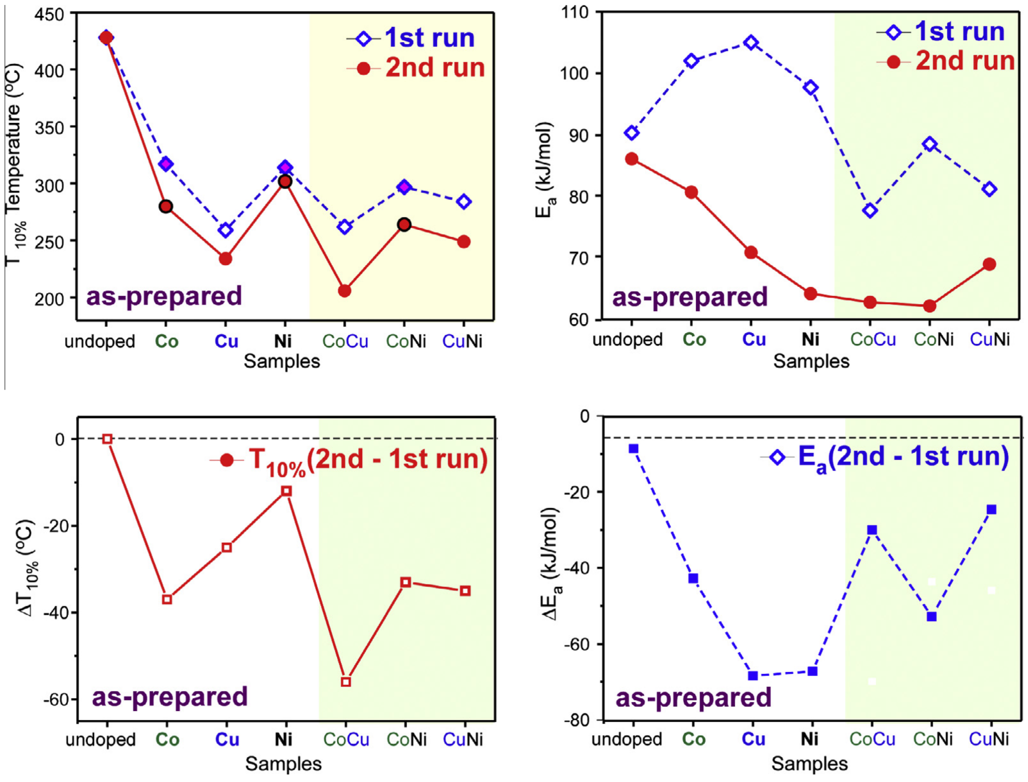

Fig. 7. $T_{10\%}$ (top left), activation energies (top right), and the difference ($T_{10\%}$ and E_a) profiles (bottom) for the first and second CO oxidation runs of reference (undoped) CeO_2, doped (Co, Cu, and Ni) and co-doped (CoCu, CoNi, and CuNi) CeO_2 catalysts.

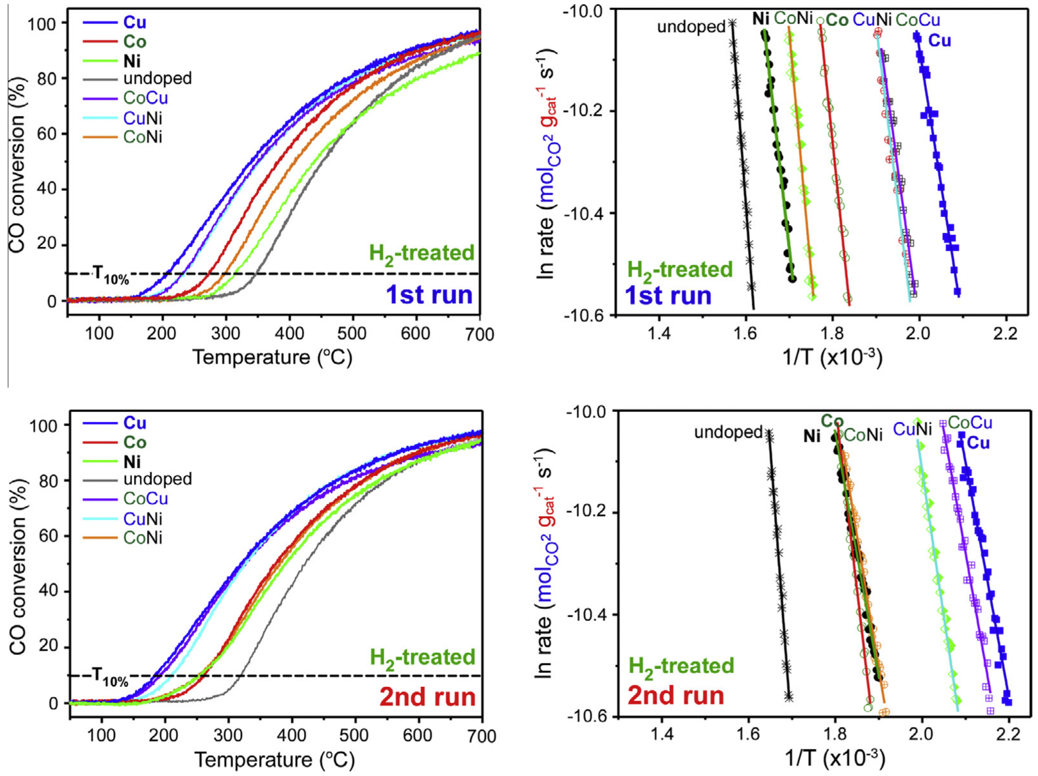

Fig. 8. Temperature programmed CO oxidation conversion (%) profiles (left two) and the corresponding Arrhenius plots (right two) for the first and second runs of H_2-treated reference (undoped) CeO_2, doped (Co, Cu, and Ni) and co-doped (CoCu, CoNi, and CuNi) CeO_2 catalysts.

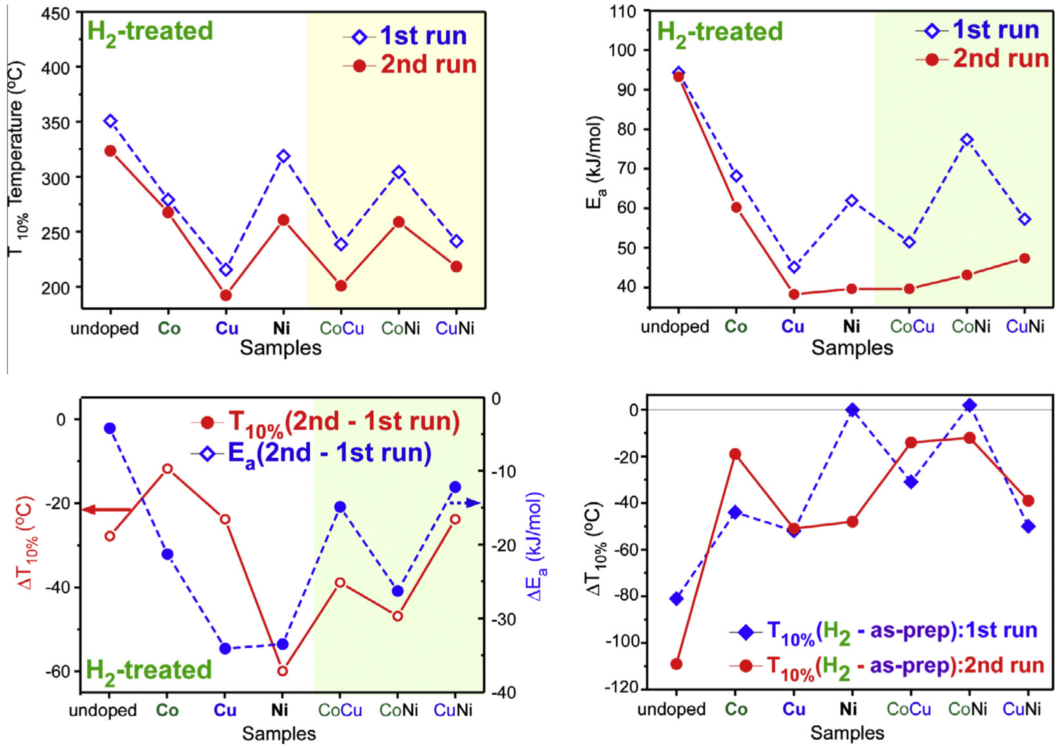

Fig. 9. $T_{10\%}$ (top left), activation energies (top right), and the difference ($T_{10\%}$ and E_a) profiles (bottom left) for the first and second CO oxidation runs of H_2-treated reference (undoped) CeO_2, doped (Co, Cu, and Ni) and co-doped (CoCu, CoNi, and CuNi) CeO_2 catalysts. Differences (bottom right) in $T_{10\%}$ between the as-prepared and H_2-treated samples for the first and second runs.

poor enhancement. In the second run, the $T_{10\%}$ was further lowered by −12 °C, −24 °C, −60 °C, −39 °C, −47 °C and 24 °C for Co, Cu, Ni, CoCu, CoNi, and CuNi-doped CeO_2 catalysts, respectively shown in Fig. 9 (bottom left). The $T_{10\%}$ (°C) occurred in the order of undoped

Table 2
Kinetic parameters for the first and second CO oxidation runs of as-prepared and of H_2-treated reference CeO_2, doped (Co, Cu, and Ni) and co-doped (CoCu, CoNi, and CuNi) CeO_2 catalysts.

Catalysts	As-prepared		H_2-treated at 450 °C	
	E_a (kJ/mol)[a] 1st/**2nd** runs	$T_{10\%}$ (°C) 1st/**2nd** runs	E_a (kJ/mol)[a] 1st/**2nd** runs	$T_{10\%}$ (°C) 1st/**2nd** runs
Undoped CeO_2	90.3/**86.1**	428/**428**	94.3/**93.2**	347/**319**
Co–CeO_2	102.0/**80.7**	317/**280**	68.2/**60.3**	273/**261**
Cu–CeO_2	105.0/**70.9**	259/**234**	45.2/**38.3**	207/**183**
Ni–CeO_2	97.7/**64.2**	314/**302**	62.0/**39.7**	314/**254**
CoCu–CeO_2	77.7/**62.8**	262/**206**	51.5/ **39.7**	231/**192**
CoNi–CeO_2	88.5/**62.2**	297/**264**	77.4/**43.2**	299/**252**
CuNi–CeO_2	81.2/**69.0**	284/**249**	57.3/**47.4**	234/**210**

[a] The activation energy was measured in the CO conversion range of 10–15%.

(347 °C) < Ni (314 °C) < CoNi (299 °C) < Co (273 °C) < CuNi (234 °C) ≈ CoCu (231 °C) < Cu (207 °C) in the first run, and undoped (319 °C) < Co (261 °C) ≈ Ni (254 °C) ≈ CoNi (252 °C) < CuNi (234 °C) ≈ CoCu (231 °C) < Cu (207 °C) in the second run. The activation energies were drastically decreased for the metal-doped CeO_2 upon thermal H_2-treatment while that of undoped CeO_2 showed no significant change. This could indicate that the interface between the doped metals and CeO_2 support plays a role in CO oxidation. The Cu-doped CeO_2 showed the most drastic change ($\Delta E_a = 60$ kJ/mol) in activation energy. In the second run, the E_a was further lowered expect for undoped CeO_2 (Fig. 9).

We selected two (undoped and Cu-doped) CeO_2 samples and thermal-treated in N_2 condition to check if reduced surface (by H_2-treatment) plays a major role in the enhancement of CO oxidation performance. Fig. 10 shows the first and second run CO conversion (%) profiles and the corresponding Arrhenius plots for the N_2-treated catalysts. For comparison, Table 3 summarized the kinetic parameters for the first and second CO oxidation runs of as-prepared, H_2-treated and N_2-treated undoped and Cu-doped CeO_2 catalysts. For the thermal N_2-treated undoped CeO_2, $T_{10\%}$ was observed at 319 °C in the first run. This value was lower by 28 °C, compared with that of thermal H_2-treated undoped CeO_2. This result implies that the enhancement of CO oxidation was not simply due to reduced surface state but due to enhanced crystallinity and/or impurity removal upon thermal treatment. In the second run, $T_{10\%}$ was somewhat increased by 8 °C, due to a slight change in crystallinity after the first run. For the N_2-treated Cu-doped CeO_2, $T_{10\%}$ was observed at 212 °C in the first run. This value

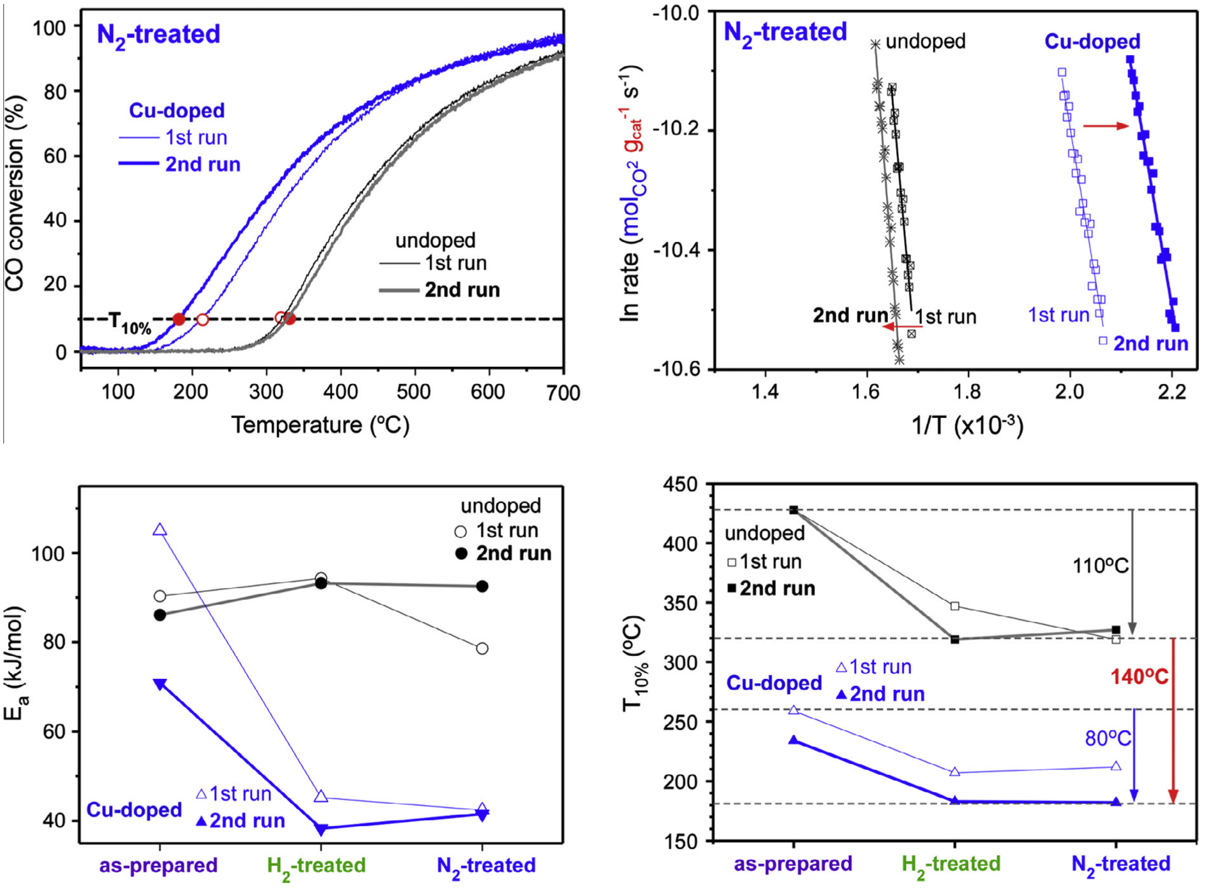

Fig. 10. $T_{10\%}$ (top left) and activation energies (top right) of thermal N_2-treated undoped CeO_2 and Cu-doped CeO_2 catalysts for the first and second CO oxidation runs. Activation energies (bottom left) and $T_{10\%}$ (bottom right) for the first and second CO oxidation runs of as-prepared, H_2-treated and N_2-treated undoped and Cu-doped CeO_2 catalysts.

Table 3
Kinetic parameters for the first and second CO oxidation runs of as-prepared, H_2-treated and N_2-treated undoped and Cu-doped CeO_2 catalysts.

Catalysts	As-prepared		H_2-treated at 450 °C		N_2-treated at 450 °C	
	E_a (kJ/mol)[a] 1st/**2nd**	$T_{10\%}$ (°C) 1st/**2nd**	E_a (kJ/mol)[a] 1st/**2nd**	$T_{10\%}$ (°C) 1st/**2nd**	E_a (kJ/mol)[a] 1st/**2nd**	$T_{10\%}$ (°C) 1st/**2nd**
Undoped CeO_2	90.3/**86.1**	428/**428**	94.3/**93.2**	347/**319**	78.6/**92.5**	319/**327**
Cu–CeO_2	105.0/**70.9**	259/**234**	45.2/**38.3**	207/**183**	42.4/**41.5**	212/**182**

[a] The activation energy was measured in the CO conversion range of 10–15%.

was comparable to that of thermal H_2-treated Cu-doped CeO_2. In the second run, $T_{10\%}$ was significantly lowered by 30 °C, and same as that of H_2-treated Cu-doped CeO_2. The activation energies of undoped CeO_2 showed negligible change upon H_2- and N_2-treatment while those of Cu-doped CeO_2 showed a drastic decrease after the thermal H_2- and N_2-treatment. Overall, the N_2-treated samples showed comparable or better CO oxidation performance than the H_2-treated samples. In other words, H_2-treatment does not lead a superior advantage than N_2-treatment. This implies that reduced surface (or reduced metal oxides) is not highly active for CO oxidation.

Since CO oxidation reactions over metal oxide catalysts have extensively been studied we here simplified CO oxidation reaction mechanism as $CO + 1/2O_2 + M\text{–}[O]\text{–}Ce\text{–}\square_{vac} \rightarrow [CO\text{–}M\text{–}O\text{–}Ce\text{–}O]^* \rightarrow CO_2\ (g) + M\text{–}[O]\text{–}Ce\text{–}\square_{vac}$, where M–[O]–Ce = metal doped in the CeO_2 support, M = doped and codoped metals, and $\square_{vac}$ = oxygen vacancy. Liu et al. [58] and Pu et al. [24] suggested that during CO oxidation on Cu–CeO_2 catalyst, CO is chemisorbed onto Cu^+ sites, after which it reacts with oxygen at the interface between CeO_2 and the doped metal, while the oxygen is activated at the oxygen vacancy site [24]. Bera et al. attributed the higher catalytic activity of Cu–CeO_2 catalyst to balanced charge pairs ($Ce^{3+} + Cu^{2+} = Ce^{4+} + Cu^+$) of Cu^{2+}/Cu^+ and Ce^{4+}/Ce^{3+} [51]. For Co and Ni-doped CeO_2 catalysts, Co^{3+}/Co^{2+} and Ni^{3+}/Ni^{2+} charge pairs will be balanced with Ce^{4+}/Ce^{3+} pairs [51,55]. However, because the redox potentials show the order of $Co^{3+}/Co^{2+} \approx Ni^{3+}/Ni^{2+} \gg Cu^{2+}/Cu^+$, the Co and Ni will be less facial than Cu to enable good balance with the Ce^{4+}/Ce^{3+} pair, resulting in poor CO oxidation performance, which is consistent with the results of the present study. Jia et al. provided solid evidence of an interfacial CO oxidation reaction [23]. Specifically, they prepared CuO (4.1 nm)/CeO_2 and CeO_2 (4.0 nm)/CuO catalysts with similar interfacial contact areas and observed the same catalytic activity. Therefore, they concluded that the perimeter of the CuO—CeO_2 interface is the active site for oxygen activation to precede CO oxidation. Adsorption of CO on doped-metal oxide is known to be important. Wang et al. showed a CO oxidation activity order of Co < Ni < Cu using CeO_2 as support, where the Ni and Co cations were less facial for CO adsorption [55,56]. The lower CO oxidation activity could also reflect good CO dissociation without associating with atomic oxygen, resulting in less CO_2 being detected [59]. The CoCu-codoped CeO_2 showed better CO oxidation performance than Co and Cu-doped CeO_2, and the CoNi-codoped CeO_2 showed better CO oxidation performance than Co and Ni-doped CeO_2. However, it is currently unclear whether the hybrid effect is due to synergy as a result of one metal being responsible for the adsorption and another for the change in balance (or oxygen defect).

4. Conclusion

To examine the metal-doping, the hybrid effects and thermal treatments on CO oxidations, we doped and co-doped transition metals (Co, Cu, and Ni) into CeO_2 support and thermal-treated in H_2 and N_2 condition. Although we could not provide the exact mechanism and the precise role of the doped metals we have obtained following important conclusions.

(1) The bandgap of undoped CeO_2 (2.88 eV) decreased to 2.0–2.4 eV upon metal doping. The BET surface areas were increased by about 1.6 (for Ni)–11.8 m^2/g (for Cu), while it was 56.4 m^2/g for undoped CeO_2. The crystallite sizes were calculated in the range from 12.3 (for Cu) to 16.1 nm (for Ni) for doped samples, which was smaller than 18.0 nm of CeO_2 using XRD patterns. It was found that the particle size (or BET surface area) was not a major factor to determine the catalytic activity.

(2) Doping and co-doping enabled lowering of the CO oxidation temperature by 126–222 °C for the as-prepared samples. The increase in catalytic activity is attributed to metal-support interactions, which is much more important than size, bulk crystal structure and surface area. The change in CO oxidation activity with temperature occurred in the order of undoped (428 °C) ≪ Co (317 °C) ≈ Ni (314 °C) < CoNi (297 °C) < CuNi (284 °C) < CoCu (262 °C) ≈ Cu (259 °C) in the first run, whereas it was undoped (428 °C) ≪ Ni (302 °C) < Co (280 °C) < CoNi (264 °C) < CuNi (249 °C) < Cu (234 °C) < CoCu (206 °C) in the second run. The enhancement of activity in the second run appears to be due to an increase in metal-support interaction. The slight difference in order (e.g., Cu and CoCu) is due to a synergic alloying effect of two different metals.

(3) The CO oxidation performance was enhanced by thermal treatment. The thermal N_2 and H_2-treatments showed similar CO oxidation performance. The thermal H_2-treatment showed no superior advantage than the thermal N_2-treatment. For the thermal H_2-treated samples, $T_{10\%}$ (°C) occurred in the order of undoped (347 °C) < Ni (314 °C) < CoNi (299 °C) < Co (273 °C) < CuNi (234 °C) ≈ CoCu (231 °C) < Cu (207 °C) in the first run, and undoped (319 °C) < Co (261 °C) ≈ Ni (254 °C) ≈ CoNi (252 °C) < CuNi (234 °C) ≈ CoCu (231 °C) < Cu (207 °C) in the second run.

The Cu-contained CeO_2 catalysts after thermal treatment commonly showed a higher catalytic activity, tentatively attributed to balanced charge pairs of Cu^{2+}/Cu^+ and Ce^{4+}/Ce^{3+} for CO oxidation reactions. We could enhance CO oxidation performance by $T_{10\%}$ = 140 °C after Cu-doping, and by 80 and 110 °C upon N_2-treatment for Cu-doped and undoped CeO_2 samples, respectively. Overall, our study provides further useful information to development of smart catalysts for a clean environment as well as chemical industry applications.

Acknowledgement

This work was financially supported by the India-Korea joint project, the National Research Foundation of Korea (NRF) grant funded by the Korean government (MEST) (2012-0006296), and the Department of Science and Technology, New Delhi through the Indo-Korea/P-02 grant.

References

[1] S. Royer, D. Duprez, ChemCatChem 3 (2011) 24–65.
[2] E.W. McFarland, H. Metiu, Chem. Rev. 113 (2013) 4391–4427.
[3] Z. Qu, F. Yu, X. Zhang, Y. Wang, J. Gao, Chem. Eng. J. 229 (2013) 522–532.
[4] S.Y. Christou, A.M. Efstathiou, Top. Catal. 42–43 (2007) 351–355.
[5] L.F. Peiretti, I.S. Tiscornia, E.E. Miro, Chem. Eng. J. 223 (2013) 507–515.
[6] A. Razeghi, A. Khodadadi, H. Ziaei-Azad, Y. Mortazavi, Chem. Eng. J. 164 (2012) 214–220.
[7] G. Yi, Z. Xu, G. Guo, K. Tanaka, Y. Yuan, Chem. Phys. Lett. 479 (2009) 128–132.
[8] G. Avgouropoulos, T. Ioannides, Chem. Eng. J. 176–177 (2011) 14–21.
[9] V. Shapovalov, H. Metiu, J. Catal. 245 (2007) 205–214.
[10] X. Nie, H. Qian, Q. Ge, H. Xu, R. Jin, ACS Nano 6 (2012) 6014–6022.
[11] Tana, F. Wang, H. Li, W. Shen, Catal. Today 175 (2011) 541–545.
[12] J. Guzman, S. Carrettin, A. Corma, J. Am. Chem. Soc. 127 (2005) 3286–3287.
[13] Y. Kang, M. Sun, A. Li, Catal. Lett. 142 (2012) 1498–1504.
[14] S. Chang, M. Li, Q. Hua, L. Zhang, Y. Ma, B. Ye, W. Huang, J. Catal. 293 (2012) 195–204.
[15] J. Zhang, L. Li, X. Huang, G. Li, J. Mater. Chem. 22 (2012) 10480–10487.
[16] P. Bera, K.C. Patil, M.S. Hegde, Phys. Chem. Chem. Phys. 2 (2000) 3715–3719.
[17] G. Mondragon-Galicia, R. Perez-Hernandez, C.E. Gutierrez-Wing, D. Mendoza-Anaya, Phys. Chem. Chem. Phys. 13 (2011) 16756–16761.
[18] J.Y. Luo, M. Meng, H. Xian, Y.B. Tu, X.G. Li, T. Ding, Catal. Lett. 133 (2009) 328–333.
[19] D.I. Potemkin, P.V. Snytnikov, V.D. Belyaev, V.A. Sobyanin, Chem. Eng. J. 176–177 (2011) 165–171.
[20] J. Qi, J. Chen, G. Li, S. Li, Y. Gao, Z. Tang, Energy Environ. Sci. 5 (2012) 8937–8941.
[21] S.M. Zhang, W.P. Huang, X.H. Qiu, B.Q. Li, X.C. Zheng, S.H. Wu, Catal. Lett. 80 (2002) 41–46.
[22] R.S. Sundar, S. Deevi, J. Nano Res. 8 (2006) 497–509.
[23] A.P. Jia, S.Y. Jiang, J.Q. Lu, M.F. Luo, J. Phys. Chem. C 114 (2010) 21605–21610.
[24] Z.Y. Pu, X.S. Liu, A.P. Jia, Y.L. Xie, J.Q. Lu, M.F. Lu, J. Phys. Chem. C 112 (2008) 15045–15051.
[25] K.Y. Ho, K.L.J. Yeung, J. Catal. 242 (2006) 131–141.
[26] K.Y. Ho, K.L.J. Yeung, Gold Bull. 40 (2007) 15–30.
[27] J.M. Zamaroa, N.C. Perez, E.E. Miro, C. Casado, B. Seoane, C. Tellez, J. Coronas, Chem. Eng. J. 195-196 (2012) 180–187.
[28] I. Luisetto, S. Tuti, E.D. Bartolomeo, Int. J. Hydrogen Energy 37 (2012) 15992–15999.
[29] C. Sun, H. Li, L. Chen, Energy Environ. Sci. 5 (2012) 8475.
[30] J. Kaspar, P. Fornasiero, M. Graziani, Catal. Today 50 (1999) 285–298.
[31] A. Trovarelli, Catal. Rev. 38 (1996) 439–520.
[32] V.P. Zhdanov, B. Kasemo, Appl. Surf. Sci. 135 (1998) 297–306.
[33] H.Y. Kim, H.M. Lee, G. Henkelman, J. Am. Chem. Soc. 134 (2012) 1560–1570.
[34] L.C. Hsu, M.K. Tsai, Y.H. Lu, H.T. Chen, J. Phys. Chem. C 117 (2013) 433–441.
[35] M.V. Ganduglia-Pirovano, A. Hofmann, J. Sauer, Surf. Sci. Rep. 62 (2007) 219–270.
[36] M. Fernandez-Garcia, A. Martinez-Arias, J.C. Hanson, J.A. Rodriguez, Chem. Rev. 104 (2004) 4063–4104.
[37] Z. Yang, G. Luo, Z. Lu, K. Hermansson, J. Chem. Phys. 127 (2007) 074704.
[38] J. Paier, C. Penschke, J. Sauer, Chem. Rev. 113 (2013) 3949–3985.
[39] Z. Yang, B. He, Z. Lu, K. Hermansson, J. Phys. Chem. C 114 (2010) 4486–4494.
[40] F. Zhang, Q. Jin, S.W. Chan, J. Appl. Phys. 95 (2004) 4319–4326.
[41] R. Rao, Q. Zhang, H. Liu, M. Yang, Q. Ling, A. Zhang, CrystEngComm 14 (2012) 5929–5936.
[42] X. Wang, Z. Jiang, B. Zheng, Z. Xie, L. Zheng, CrystEngComm 14 (2012) 7579–7582.
[43] F. Dang, K. Kato, H. Imai, S. Wada, H. Haneda, M. Kuwabara, Cryst. Growth Des. 10 (2010) 4537–4541.
[44] S. Yang, L. Gao, J. Am. Chem. Soc. 128 (2006) 9330–9331.
[45] W. Shi, Y. Li, J. Hou, H. Lv, X. Zhao, P. Fang, F. Zheng, S. Wang, J. Mater. Chem. A 1 (2013) 728–734.
[46] M. Taguchi, S. Takami, T. Adschiri, T. Nakane, K. Sato, T. Naka, CrystEngComm 13 (2011) 2841–2848.
[47] R. Perez-Hernandez, G. Mondragon-Galicia, A.A. Maravilla, J. Palacios, Phys. Chem. Chem. Phys. 15 (2013) 12702–12708.
[48] W. Xu, Z. Liu, A.C. Johnston-Peck, S.D. Senanayake, G. Zhou, D. Stacchiola, E.A. Stach, J.A. Rodriguez, ACS Catal. 3 (2013) 975–984.
[49] H. Song, B. Tan, U.S. Ozkan, Catal. Lett. 132 (2009) 422–429.
[50] M.S. Yakimova, V.K. Ivanov, O.S. Polezhaeva, A.A. Trushin, A.S. Lermontov, A.Y.D. Tretyakov, Dokl. Chem. 427 (2009) 186–189.
[51] P. Bera, S. Mitra, S. Sampath, M.S. Hegde, Chem. Commun. (2001) 927–928.
[52] X. Wang, J.A. Rodriguez, J.C. Hanson, D. Gamarra, A. Martinez-Arias, M. Fernandez-Garcia, J. Phys. Chem. B 110 (2006) 428–434.
[53] Y. Liu, T. Hayakawa, T. Tsunoda, K. Suzuki, S. Hamakawa, K. Murata, R. Shiozaki, T. Ishii, M. Kumagai, Top. Catal. 22 (2003) 205–213.
[54] Z. Wu, M. Li, J. Howe, H.M. Meyer III, S.H. Overbury, Langmuir 26 (2010) 16595–16606.
[55] S.Y. Wang, N. Li, L.F. Luo, W.X. Huang, Z.Y. Pu, Y.J. Wang, G.S. Hua, M.F. Luo, J.Q. Lu, Appl. Catal. B 144 (2014) 325–332.
[56] A.P. Jia, G.S. Hu, L. Meng, Y.L. Xie, J.Q. Lu, M.F. Luo, J. Catal. 289 (2012) 199–209.
[57] H.V. Fajardo, L.F.D. Probst, N.L.V. Carreño, I.T.S. Garcia, A. Valentini, Catal. Lett. 119 (2007) 228–236.
[58] W. Liu, A.F. Sarofim, M. Flytzani-Stephanopoulos, Chem. Eng. Sci. 49 (1994) 4871–4888.
[59] S. Tang, J. Lin, K.L. Tan, Catal. Lett. 51 (1998) 169–175.